

Mid/far-infrared semiconductor devices exploiting plasmonic effects

R. Colombelli^{*,a}, Y. Chassagneux^a, A. Bousseksou^a, V. Moreau^a,
S. Barbieri^b, C. Sirtori^b, G. Patriarche^c, G. Beaudoin^c, I. Sagnes^c, H.E. Beere^d, D.A. Ritchie^d

^a Institut d'Electronique Fondamentale, Université Paris Sud and CNRS, UMR 8622, 91405 Orsay, France

^b Laboratoire MPQ, Université Paris-VII and CNRS, UMR 7162, 75013 Paris, France

^c CNRS/LPN, Laboratoire de Photonique et de Nanostructures, Route de Nozay, 91460 Marcoussis, France

^d Cavendish Laboratory, University of Cambridge, Cambridge CB3 0HE, United Kingdom

Abstract

We show how metallic waveguides offer the opportunity of implementing interesting functionalities for semiconductor lasers within a simple technological approach. In the THz, we show that the active region thickness of quantum cascade lasers can be reduced by a factor of 2 without effects on the threshold current density and maximum operating temperature of the laser. Pulsed and continuous-wave operation – with a low threshold $J_{th} = 71 \text{ A/cm}^2$ – are obtained for a $5.86\text{-}\mu\text{m}$ -thick THz QC laser. The emission is peaked at $\lambda \approx 115 \text{ }\mu\text{m}$ and the waveguide resonator is based on a metal-metal geometry. In the mid-infrared, we demonstrate surface-plasmon distributed-feedback quantum cascade lasers with a first-order grating realised by the sole patterning the top metallic contact. The devices have a single mode emission with a side-mode suppression ratio greater than 20dB. The emission wavelength at 78K is centred at $\lambda = 7.3 \text{ }\mu\text{m}$ and has tuning rate as a function of the temperature of $\approx 0.4 \text{ nm/K}$.

Keywords: Mid-infrared, THz, quantum cascade lasers, surface-plasmons

1. INTRODUCTION

THz quantum cascade (QC) lasers are semiconductor-based pulsed- and continuous-wave (cw) sources of coherent radiation covering the frequency range between 1.9 and 5 THz ($\lambda \approx 60\text{--}160 \text{ }\mu\text{m}$) [1,2]. Currently, the best temperature performance has been obtained using resonators where the mode confinement is provided by a double-sided metal waveguide [3,4,5], mostly because of their improved thermal properties. The main drawbacks of this waveguide geometry are the low power extraction and poor beam quality [6], both a consequence of the sub-wavelength radiation confinement [7]. However, contrary to standard dielectric or even one-sided surface plasmon waveguides, extensively used for mid-infrared (mid-IR) and THz QCLs, metal-metal waveguides offer the opportunity of reducing to a minimum the active-region (AR) thickness without sacrificing the confinement factor, which remains always close to unity [8].

In the mid-infrared, the QC laser is an ideal semiconductor source. For applications such as gas sensing and high resolution spectroscopy, single-mode operation of the devices is often required [9]. The architecture of choice to achieve single-mode emission is the use of gratings for distributed-feedback (DFB). Advances in the design and technology of QC lasers have led to the demonstration of single-mode operation at room temperature at several wavelengths [10,11,12]. The typical strategy to realise these single-mode lasers is to integrate a buried DFB grating within a Fabry-Perot QC laser.

In this paper, we will demonstrate how the peculiarity of metallic surface-plasmon waveguides allows one to develop novel functionalities for THz and mid-infrared QC lasers.

2. APPLICATIONS TO DEVICES OPERATING IN THE THZ RANGE

2.1 THz QC lasers with thin active cores

For THz QC lasers, the propagation losses increase when the AR is thinner due to a stronger mode penetration into the metal layers, but if thin contact layers are employed ($\approx 100/200 \text{ nm}$) the losses can be kept reasonably low, as it is shown in Fig. 1. From the figure we can predict an increase of the total losses ($\alpha_{\text{mirror}} + \alpha_{\text{waveguide}}$) of approximately 40/50 % when

the active region is reduced from $\approx 12 \mu\text{m}$ to $\approx 6 \mu\text{m}$. The mirror losses are $\approx 0.93 \text{ cm}^{-1}$ and $\approx 1.85 \text{ cm}^{-1}$, for AR thicknesses of $6 \mu\text{m}$ and $12 \mu\text{m}$ respectively, as deduced from Ref. [6].

We demonstrate THz QC lasers with an AR thickness of $5.86 \mu\text{m}$, i.e. approximately a factor of two lower than the typical thickness used so far [4-6]. Despite this considerable reduction in thickness, the performance in terms of threshold current density (J_{th}) and maximum operating temperature (T_{max}) does not degrade. Devices that feature reduced-thickness active regions are interesting for several reasons. First, a thickness reduction eases the semiconductor growth, as $10\text{-}\mu\text{m}$ (or more) -thick epitaxial layers already push MBE technology to its limit, and – in the long term – could represent an obstacle to device commercialization. Secondly, the operating bias scales linearly with the active region thickness and allows one to limit the *total injected electrical power* in the structure. Finally, the stronger mode penetration into the metal layers could ease the implementation of strongly-coupled 1-st and 2-nd order gratings by the sole patterning of the top metallic contacts.

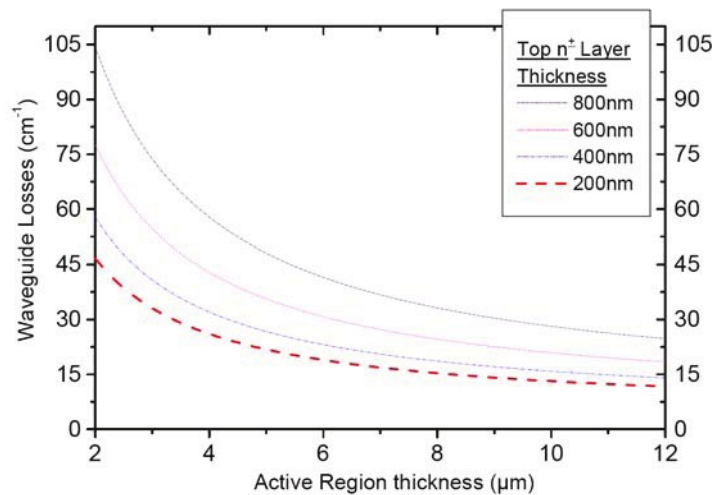


Fig. 1. Waveguide losses (α_w) as a function of the active region thickness for a typical metal-metal waveguide and for several different thicknesses of the top n^+ -GaAs contact layer. The thickness and doping of the bottom contact layer are 80 nm and $5 \times 10^{18} \text{ cm}^{-3}$, respectively.

2.2 Sample structure and growth

The sample was grown by molecular-beam epitaxy, with active region thickness of $5.86 \mu\text{m}$ (45 active region/injector stages, sample V298). The active region, designed for emission at 2.9 THz (12 meV) is described in Ref. [13], and is sandwiched between 700 nm , $2 \times 10^{18} \text{ cm}^{-3}$ and 80 nm , $5 \times 10^{18} \text{ cm}^{-3}$ doped layers forming the lower and upper contacts.. Two quantum wells in the injector superlattice were n-doped at levels of $1.3 \times 10^{16} \text{ cm}^{-3}$, while in Ref. [13] the doping level was $1.6 \times 10^{16} \text{ cm}^{-3}$. This doping reduction does not have a dramatic effect, but helps reducing the losses by a few cm^{-1} . Finally, a 300-nm -thick $\text{Al}_{0.50}\text{Ga}_{0.50}\text{As}$ etch stop layer was grown between the substrate and the lower contact layer.

2.3 Sample processing

The sample was processed in both standard and metal-metal waveguide configurations. In the former case, the lasers were wet etched into ridge cavities $100/160/220/320 \mu\text{m}$ wide, and $6 \mu\text{m}$ deep. Ni/Ge/Au/Ni/Au contacts were used as top and bottom metallization. In the latter case (metal-metal waveguide), the active region was first thermo compressively bonded (Au-Au bonding) on top of an n^+ GaAs host substrate, and the original semi-insulating substrate removed by wet etching. Subsequently the n^+ -GaAs top contact was thinned from 700 nm to 200 nm to reduce the losses (see Fig. 1) and laser ridges were fabricated by wet-etching with the same procedure as above. The devices were cleaved into laser bars ($\approx 2 \text{ mm}$ long), indium soldered to copper blocks, wire bonded, and mounted in a continuous flow liquid helium cryostat for device characterizations.

2.4 Measurements and results

The experimental results for wafer V298 (5.86 μm thick AR) are reported in Figs. 2 and 3. Devices from this *same* wafer were fabricated using the metal-metal (Fig. 2) and also the single-surface-plasmon waveguide geometry (Fig. 3). In the former case the J_{th} at 6K in cw mode is 71 A/cm^2 , and the T_{max} is 60K. In pulsed mode (data not shown) the T_{max} increases to 75K, while the J_{th} at 6K remains unchanged. These values represent low threshold current densities and reasonably high T_{max} for this type of active region with metal-metal waveguides [14], demonstrating that it is indeed possible to reduce the epitaxial thickness of THz QC lasers without compromising the performance. The results also suggest that further thickness reductions should be possible.

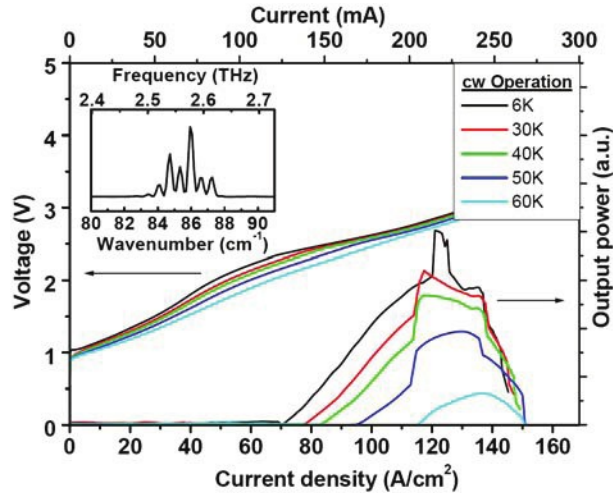


Fig. 2. L-I-V characteristic (cw) for a typical 6- μm -thick (V298) THz QC laser with a metal-metal waveguide. The device is 89 μm wide and 2 mm long. Inset: Typical spectrum at 4K for a current $I=209$ mA.

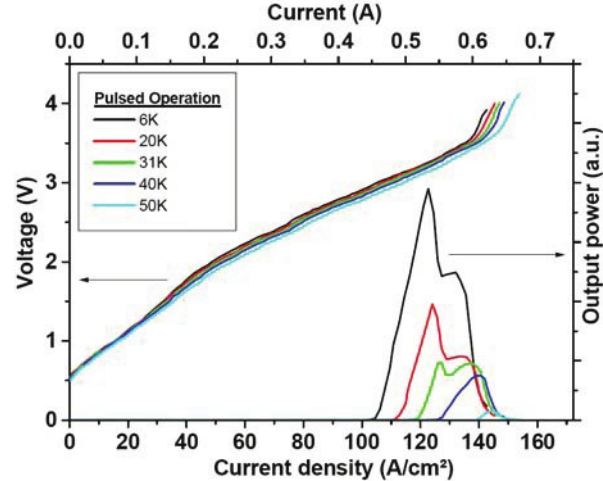


Fig. 3. L-I-V characteristic (pulsed mode) for a typical 6- μm -thick (V298) THz QC laser processed in a single-plasmon ridge waveguide configuration. The device is 216 μm wide and 2 mm long.

When the same wafer is processed as a single-surface-plasmon (Fig. 3), the calculated confinement factor drops from 99% to 17.5%, and the computed waveguide losses drop too from $\approx 20 \text{ cm}^{-1}$ to $\approx 5 \text{ cm}^{-1}$. If the mirror losses for a 2-mm-long ridge are taken into account ($\alpha_{\text{mirror}} \approx 5.6 \text{ cm}^{-1}$), a decrease of the theoretical figure of merit of almost 2.9 times (from 49 to 17) is expected for the single-surface-plasmon device. The experimental results agree only qualitatively with the simulations. Indeed, from Fig. 3 we report a J_{th} of 104 A/cm^2 in pulsed operation at 6K, which represents an increase of only 40% with respect to the metal-metal waveguide. However the T_{max} is only 50K in pulsed mode. As explained in

Ref. [15], it is possible that the predicted J_{th} does not match the experimental value because a parasitic current is present between consecutive active regions at low bias, as suggested by the soft turn-on of the IVs. As a consequence, J_{th} is offset compared to its “loss controlled” value. This is a common problem for THz QC lasers [4, 15], and it makes the direct comparison of the threshold current densities quite difficult.

To support this conclusion we note that typical J_{th} measured at 4K for a 12 μm thick AR processed in a single plasmon (see Ref. [13]) or metal-metal geometry (unpublished data) are of the order of 80/100 A/cm², i.e. comparable to those found here, when, according to the computed figure of merit we would expect a decrease in J_{th} by at least 40/50 % compared to a 6 μm thick AR. Although in the present structure the doping level in the active region is slightly lower ($1.3 \times 10^{16} \text{ cm}^{-3}$ compared to $1.6 \times 10^{16} \text{ cm}^{-3}$), thus reducing the propagation losses (see Fig. 1), the doping reduction alone cannot explain the low J_{th} values that we observe in the thin-AR devices.

3. APPLICATIONS TO DEVICES OPERATING IN THE MID-INFRARED RANGE

3.1 Surface-plasmon DFB lasers

The typical strategy to realise high-performance single-mode lasers is to integrate a buried DFB grating within a Fabry-Perot QC laser. We demonstrate a different approach making use of surface-plasmon devices [18]. Single-mode long-wavelength surface-plasmon QC lasers have been demonstrated in the past at $\lambda \approx 17 \mu\text{m}$ [19]. In that case a two-metal grating was deposited, which produces a strong complex index contrast due to the large spatial modulation of the skin depth. We show here that a pure one-metal-grating, alternating metal- and air-claddings as in Fig. 4a, can operate as a frequency-selecting filter and yields single-mode operation. The advantage is in the technological simplification, since there is no need for epitaxial overgrowth or semiconductor etching. Furthermore, there are ample margins for performance improvement.

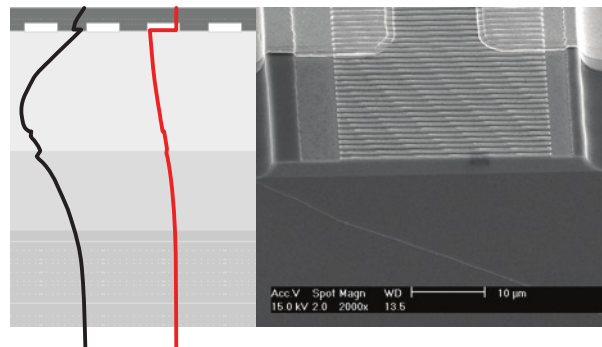


Fig. 4. (a) Schematics of the DFB devices with the distributed-feedback implemented *via* metal patterning only. The red lines sketch the waveguide modes of a full surface-plasmon and air-guided QC laser, respectively. (b) SEM image of the edge of a typical device. The lighter region, approximately 3 micron thick, corresponds to the active-region and bottom InGaAs cladding. The metallic grating is clearly visible. Its period is $\Lambda=1.15 \mu\text{m}$, with a 50% duty cycle.

3.2 Growth and device fabrication

The samples were grown in a vertical-reactor, low-pressure MOVPE system (TurboDisc D180) using hydrogen as carrier gas and standard precursors (arsine (AsH_3), phosphine (PH_3), trimethylindium (TMI), trimethylgallium (TMGa) and trimethylaluminium (TMAI)). Our growth conditions lead to an InGaAs and an InAlAs growth rate of around 1.8 ML/s for the active region. The sample contains 50 repeats of the following four-well active region+injector structure (beginning with the injection barrier, layer thicknesses in nm): **4.3**/1.7/**1.0**/5.3/**1.2**/5.2/**1.2**/4.4/**2.5**/3.1/**1.7**/2.9/**1.6**/2.7/**1.8**/2.6/**2.1**/2.6/**2.4**/2.4, where bold numbers refer to $\text{Al}_{0.52}\text{In}_{0.48}\text{As}$ barriers, roman type to $\text{In}_{0.53}\text{Ga}_{0.47}\text{As}$ wells, and the underlined layers are n-doped to $1 \times 10^{17} \text{ cm}^{-3}$. The stack of active regions+injectors is sandwiched between doped thin, top InGaAs contact facilitating layers and bottom 0.5- μm -thick InGaAs cladding layer, n-doped $5 \times 10^{16} \text{ cm}^{-3}$.

The first processing step is the metallic-grating deposition. E-beam lithography and a lift-off process have been used to deposit 50%-duty-cycle, Ti/Au (3/200-nm-thick) gratings with different periods ($\Lambda=1.15, 1.17, 1.20, 1.22$ and $1.25 \mu\text{m}$).

The gratings are typically 25 μm wide and a few millimetres long. Ridge waveguide resonators were then fabricated around the metallic gratings by contact optical lithography and wet etch. A SiN layer (300-nm-thick) was used to provide electrical insulation. After opening of the insulating layer on top of the laser ridges through reactive ion etching, lateral Ti/Au contacts were deposited by e-beam evaporation in order to contact the grating sides. Following polishing and back contact deposition, the devices were cleaved, mounted on copper blocks, bonded and loaded into a cryostat for the measurements. Fig. 4b shows a scanning electron microscope image of the edge of a typical device. For this demonstration the ridge top widths were much larger than the grating width.

3.3 Device Characterization

The lasers were tested in pulsed mode (50ns pulse width, 84 kHz repetition rate). A mercury cadmium telluride (MCT) detector was used for the light-current characterizations and spectral analysis. A current-voltage characteristic at 78 K of a typical device with grating period $\Lambda=1.15 \mu\text{m}$ is shown in Fig. 2. The threshold voltage is $\approx 14 \text{ V}$, in good agreement with the calculated design bias (14.7 V) [18]. Fig. 5 shows that the onset of lasing occurs at a current of $\approx 0.8 \text{ A}$ at a temperature of 78K, corresponding to a threshold current density $J_{\text{th}} \approx 2.6 \text{ kA/cm}^2$. This is a rather high value, but it is comparable to what is usually obtained for standard Fabry-Perot surface-plasmon QC lasers with gold plasmon-carrying layers [18]. The maximum output peak power – at 78K – from a 750 μm -long device is $\approx 65\text{mW}$. The power is reported without any correction due to the collection efficiency, which we estimate to be $\leq 50\%$.

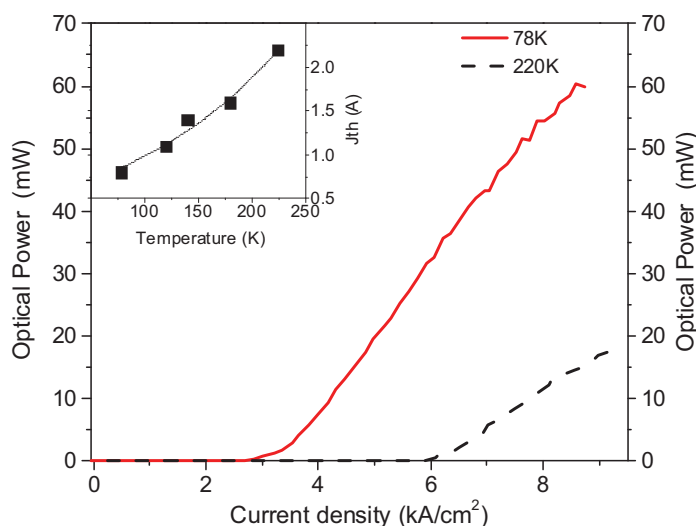


Fig. 5: L-I-V characteristic of a 750 μm X 45 μm device (25 μm -wide grating). Inset: Current threshold as a function of the heat-sink temperature.

The emission spectra are single mode for a limited current range above threshold, as shown in Fig. 6. The side-mode suppression ratio is at least 20 dB, and the tuning rate is $\approx 0.4 \text{ nm/K}$ (see Fig. 6, right inset). This latter value is 3.5 times lower than what obtained on Fabry-Perot devices fabricated from the same material, further proving the distributed origin of the feedback in these structures. Additional modes arise at higher currents, but only one or two lateral modes appear and never a Fabry-Perot like spectrum is recovered.

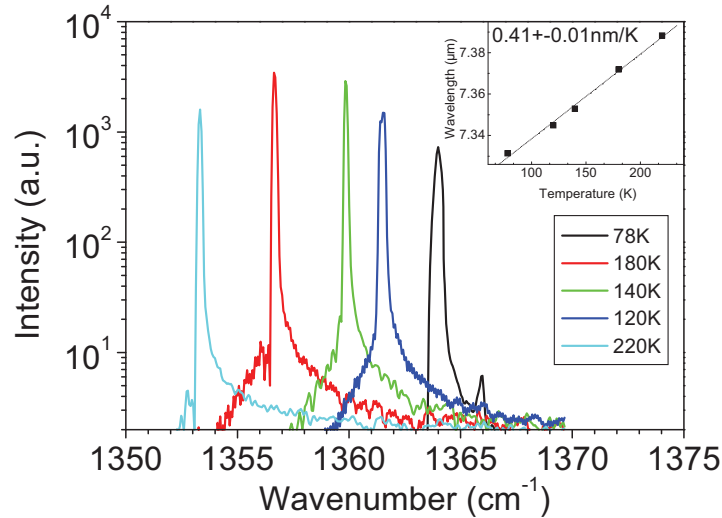


Fig. 6: Typical laser spectra of a device for different temperatures of the heat-sink. Inset: Emission wavelength as a function of the heat-sink temperature, showing a tuning rate of ≈ 0.4 nm/K.

3.4 Conclusions

We demonstrated single-mode emission from surface-plasmon QC lasers, where the distributed-feedback is achieved *via* the implementation of a metal grating in the sole patterning of the top metal contacts. The devices exhibit a >20 dB side-mode suppression ratio, and a tuning rate of ≈ 0.4 nm/K. The DFB devices have similar J_{th} as typical surface-plasmon QC lasers without grating and with Ti/Au plasmon-carrying layers, but the maximum operating temperature is lower ($T_{max} \approx 225$ K vs 265K), possibly due to the non-optimised geometry of the devices. The performances need to be improved. Major improvements are expected from (i) process optimization, by reducing the size difference between the grating and the ridge width, and (ii) grating duty-cycle reduction. Initial theoretical results suggest in fact that modes with very low propagation losses can appear if the grating duty-cycle is reduced. This is not only related to the reduction of the surface covered by metal, but also to a coupling mechanism between surface-plasmon and air-guided modes (see scheme in Fig. 4a). This latter mechanism is reminiscent of the effect described in Ref. [20]. We believe that this technology offers the opportunity of an extremely simple implementation of single-mode DFB lasers, for applications that require device operation in pulsed mode.

4. ACKNOWLEDGEMENTS

We thank F. Julien, M. Carras, S. Laurent, S. Dhillon, J. Teissier for help and discussions. The device fabrication has been performed at the nano-center CTU-IEF-Minerve which was partially funded by the “Conseil Général de l'Essonne”. We gratefully acknowledge support from ANR-06-NANO-047 “MetalGuide”. This work was conducted as part of a EURYI scheme award. See www.esf.org/euryi.

REFERENCES

- * Email: raffaele.colombelli@u-psud.fr
- [1] Kohler R., Tredicucci A., Beltram F., Beere H.E., Linfield E.H., Davies A.G. Davies, Ritchie D.A., Iotti R.C., Rossi F., “Terahertz semiconductor-heterostructure laser”, *Nature* **417**, 156 (2002).
- [2] Kumar S., Williams S., Hu Q., Reno J.L., “1.9 THz quantum-cascade lasers with one-well injector”, *Appl. Phys. Lett.* **88**, 121123 (2006).
- [3] Unterrainer C., Colombelli R., Gmachl C., Capasso F., Hwang H., Sivco D.L., Cho A.Y., “Quantum Cascade Lasers with Double Metal-Semiconductor Waveguide Resonators”, *Appl. Phys. Lett.* **80**, 3060 (2002).

- [4] Williams B., Kumar S., Callebaut H., Hu Q., Reno J., "Terahertz quantum-cascade laser at $\lambda=100\text{ }\mu\text{m}$ using metal waveguide for mode confinement," *Appl. Phys. Lett.* **83**, 2124 (2003).
- [5] Williams B., Kumar S., Hu Q., Reno J., "Operation of terahertz quantum-cascade lasers at 164 K in pulsed mode and at 117 K in continuous-wave mode," *Optics Express* **13**, 3331 (2005).
- [6] Kohen S., Williams B.S., Hu Q., "Electromagnetic modeling of terahertz quantum cascade laser waveguides and resonators", *J. Appl. Phys.* **97**, 053106 (2006).
- [7] E.E. Orlova, et al., « Antenna model for wire lasers », *Phys. Rev. Lett.* **96**, 173904-1 (2006).
- [8] Gmachl C., Capasso F., Tredicucci A., Sivco D.L., Kohler R., Hutchinson A.L., Cho A.Y., "Dependence of the Device Performance on the Number of Stages in Quantum-Cascade Lasers", *IEEE J. Sel. Topics Quantum. Electron.* **5**, 808 (1999).
- [9] Kosterev, A. et al., 'Chemical sensors based on quantum cascade lasers' *IEEE J. Quantum Electron.* **38**, 582 (2002).
- [10] Lee, B.G. et al., 'Widely tunable single-mode quantum cascade laser source for mid-infrared spectroscopy', *Appl. Phys. Lett.* **91**, 231101 (2007).
- [11] Darvish, S.R. et al., 'High-power, continuous-wave operation of distributed-feedback quantum-cascade lasers at $\lambda\approx 7.8\text{ }\mu\text{m}$ ', *Appl. Phys. Lett.* **89**, 251119 (2006).
- [12] Blaser, S. et al., 'Room-temperature, continuous-wave, single-mode quantum-cascade lasers at λ similar or equal to $5.4\text{ }\mu\text{m}$ ' *Appl. Phys. Lett.* **86**, 041109 (2005).
- [13] Barbieri S., Alton J., Beere H.E., Fowler J., Linfield E.H., Ritchie D.A., "2.9 THz quantum cascade lasers operating up to 70 K in continuous wave", *Appl. Phys. Lett.* **85**, 1674 (2004).
- [14] J. Alton, S.S. Dhillon, C. Sirtori, A. de Rossi, M. Calligaro, S. Barbieri, H.E. Beere, E.H. Linfield, D.A. Ritchie, "Buried waveguides in terahertz quantum cascade lasers based on two-dimensional surface plasmon modes", *Appl. Phys. Lett.* **86**, 071109 (2005).
- [15] J. Alton, S. Barbieri, C. Worrall, M. Houghton, H.E. Beere, E.L. Linfield, D.A. Ritchie, "Optimum resonant tunnelling injection and influence of doping density on the performance of thz bound-to-continuum cascade lasers", *SPIE Proceedings* **5727**, 65 (2005).
- [16] Y. Chassagneux, R. Colombelli, W. Maineult, S. Barbieri, H. E. Beere, D. A. Ritchie, S. P. Khanna, E. H. Linfield, A. G. Davies, "Electrically-pumped photonic-crystal, terahertz lasers controlled by boundary conditions", *Nature*, *in press* (2008).
- [17] L. Sirigu, r. Terazzi, M.I. Amanti, M. Giovannini, J. Faist, L.A. Dunbar, R. Houdré, "Terahertz quantum cascade lasers based on two-dimensional photonic crystal resonators", *Opt. Expr.* **16**, 5206-5217 (2008).
- [18] Bahriz, M. et al., Room-temperature operation of $\lambda\approx 7.5\text{ }\mu\text{m}$ surface-plasmon quantum cascade lasers ', *Appl. Phys. Lett.*, **88** 181103 (2006).
- [19] Tredicucci, A. et al., 'Single-mode surface-plasmon laser', *Appl. Phys. Lett.* **76**, 2165 (2000).
- [20] Carras, M. et al, 'Photonic modes metallodielectric periodic waveguides in the midinfrared spectral range', *Physical Review B*, **74**, 235120 (2006).